Chapter 5

Multifractality in ^{28}Si-Ag/Br Interaction at 14.5A GeV

5.1 Introduction

It is known that the theory of fractals has the ability to explain deterministic chaos in nonlinear physics [1]. Studies of intermittent behavior in turbulent fluids have also been well explained in terms of the fractal dimensions [2]. This observation has prompted the fractal formalism to be adopted to explain multiparticle emission data in high-energy collisions, which subsequently leads to the study of intermittency from the perspective of (multi)fractality. Several techniques based on the fractal theory are available to analyze the multiparticle emission data [2–4]. The most popular one has been the frequency moment method [5, 6] followed by a similar technique introduced in ref. [7]. In this chapter we use both of these methods to analyze shower track emission data of ^{28}Si-Ag/Br interaction at an incident energy of 14.5A GeV, along with a couple of detrended techniques, namely the multifractal detrended fluctuation analysis (MF-DFA) method [8] and the multifractal detrended moving average (MF-DMA) method [9].

The single particle density distribution of particles produced in a high-energy collision exhibits random fluctuations consisting of sharp peaks and deep valleys, which are apparently

devoid of any regular pattern. In the intermittency analysis we have characterized these fluctuations in terms of a set of regularly behaving parameters. The power law scaling behavior of SFM as elucidated in Eq. (3.23) indicates that some kind of scale invariant dynamics is involved in the particle production process that may have a connection with the theory of fractals [5, 10–13]. Efforts have been made to interpret the intermittency parameters and the self-similarity observed in the particle density distribution, in terms of several conventional as well as exotic speculative processes, but each with a limited degree of success. Both the experimental and phenomenological development of the subject has been comprehensively reviewed in ref. [14].

For a self-similar process, the multifractal G_q moment (also called the frequency moment) introduced in ref. [5, 6] exhibits a power-law dependence on the phase space resolution size in a way similar to Eq. (3.23). Over intermittency the G_q moment technique has an added advantage in the sense that, by using the G_q moments one can study not only the spikes (for $q > 0$) but also the non-empty valleys (for $q < 0$), while the F_q moments are useful only for the spikes of the density distribution. Unlike the F_q moments, the G_q moments can be defined for fractional as well as for negative q values, and hence one can enjoy the freedom of computing a continuous spectrum of moments. However, in low multiplicity events as the empty bin effects dominate the G_q moments saturate with $\delta X \to 0$, and the statistical noise present in the density function cannot be automatically accounted for. The limiting condition $\delta X \to 0$ is again a mathematical idealization, and the only achievable limit is up to the phase space resolution allowed by the detector granularity. In G_q technique the noise has to be eliminated by using an equivalent uncorrelated event sample generated by the random numbers. Takagi's T_q moments on the other hand, are defined only for positive integer order q, and are not particularly affected by the finiteness of the event multiplicity [7]. Takagi used his technique to determine several multifractal parameters by analyzing $p\overline{p}$ and e^-e^+ annihilation data. However, a proper method of eliminating the statistical noise from the T_q moments has not yet been formulated. In the recent past both Hwa's and Takagi's methods have been applied to analyze high-energy nucleus-nucleus (AB) collision data at different collision energies involving different colliding systems [5, 6, 15, 16].

The multifractal detrended fluctuation analysis (MF-DFA) [8] method is a very useful tool for the multifractal characterization of noisy and nonstationary time series data. As a robust and powerful technique for capturing the long-range correlations in time series data, the method has so far been applied to various fields of stochastic analysis e.g., in stock markets, foreign exchange, geophysical time series, medicine and many more. To illustrate the applicability of the MF-DFA method we cite a few resent articles in ref. [17], certainly the list is not a complete one. In the recent past Zhang et al. [18] have applied the method probably for the first time to analyze the multiparticle data on Au+Au interaction at

$\sqrt{s_{NN}}$ =200 GeV. The multifractal detrended moving average analysis (MF-DMA) technique [9] on the other hand, is a comparatively new method adopted in time series analysis. The MF-DMA analysis method is also an efficient tool for the detection and characterization of multifractal scaling and long-range correlation properties of noisy and non-stationary time series data [19, 20]. It is obvious that like other multifractal techniques, MF-DMA technique can also be used to investigate the scale invariance property of the particle density in high-energy collisions, though to the best of our knowledge it has not so far been applied to any such multiparticle distribution.

As mentioned above, the intermittency analysis of our AB data signals towards the possibility of some kind of scale invariant dynamics that ultimately leads to a self-similar density distribution in one dimensional density distribution [21], and a self-affine distribution in the two-dimensional (η, φ) plane [22]. These observations encouraged us to perform a multifractal analysis of the ^{28}Si-Ag/Br data. Therefore, in this chapter we examine the scaling behavior of various multifractal moments and derive several parameters related to multifractality. We adopt four different techniques, namely Hwa's moment [5, 6, 11], Takagi's moment [7], the MF-DFA moment [8] and the MF-DMA moment [9]. Moreover, the results obtained from the experimental data sample are systematically compared with the predictions of the UrQMD and UrQMD+BEC simulations.

5.2 Hwa's Moment

The frequency moment or the qth order multifractal moment G_q averaged over many events as well as over many non-overlapping phase space intervals of equal size say $\delta X_\eta = \Delta X/M$, is defined as [5],

$$\langle G_q \rangle = \frac{1}{N_{ev}} \sum_{e=1}^{N_{ev}} \sum_{m=1}^{M} \left[\frac{n_m^e}{n_s^e} \right]^q . \tag{5.1}$$

In the above definition of G_q, the order q can be any real number, M represents the total number of equal size intervals into which the entire accessible phase space ΔX is partitioned, n_m^e is the number of shower tracks falling within the mth such interval of the eth event, n_s^e is the total number of shower tracks in the eth event (i.e., $n_s^e = \sum_{m=1}^{M} n_m^e$). For finite n_s^e the single event G_q moments are subjected to large statistical fluctuations that can be minimized through event averaging. To get rid of the saturation problem mentioned above, Hwa and Pan [6] introduced a step function $\Theta(n_m^e - q)$ into the definition of G_q which acts like a filter for the empty bin. With this modification the $\langle G_q \rangle$ moment is redefined as,

$$\langle G_q \rangle = \frac{1}{N_{ev}} \sum_{e=1}^{N_{ev}} \sum_{m=1}^{M} \left[\frac{n_m^e}{n_s^e} \right]^q \Theta(n_m^e - q). \tag{5.2}$$

The Θ function equals to 1 if $n_m^e > q$, and vanishes otherwise. According to the theory of fractals, if the single particle density distribution possesses multifractal structure, then $\langle G_q \rangle$ like the SFM should also exhibit a scaling relation,

$$\langle G_q \rangle \propto (\delta X_\eta)^{\tau(q)} \quad : \text{ as } \delta X_\eta \to 0. \tag{5.3}$$

The exponent $\tau(q)$ is called the 'multifractal mass exponent' or simply the 'fractal exponent' that can be related to the generalized Renyi (fractal) dimensions D_q through the relation: $\tau(q) = (q-1)\, D_q$. The phase space variable used here is nothing but the cumulative variable X_η defined in Eq. (3.22) corresponding to the pseudorapidity (η). We have calculated the G_q moments as functions of phase space partition number M over a wide range of q values. Fig. 5.1 shows the corresponding schematic representations, where $\ln \langle G_q \rangle$ has been plotted against $\ln M$ (a) for the experiment, (b) for the UrQMD, and (c) for the UrQMD+BEC. The diagrams show that the phase space dependence of G_q is more or less similar for all the three data samples e.g., $\ln \langle G_q \rangle$ increases for $q < 0$ and decreases for $q > 1$, $\ln \langle G_q \rangle$ tends to saturate at large $\ln M$, and the saturation effect that might simply be an outcome of the finiteness of $\langle n_s \rangle$, is more prominent for the higher positive values of $q(\geqslant 4)$. The mass exponent $\tau(q)$ is calculated from the linear dependence of $\ln \langle G_q \rangle$ on $\ln \delta X_\eta$ (see Eq. (5.3)) through

$$\tau(q) = \lim_{\Delta \to 0} \frac{\Delta \ln \langle G_q \rangle}{\Delta \ln \delta X_\eta}. \tag{5.4}$$

For each q, $\tau(q)$ is extracted from the best linear fit to the $\ln \langle G_q \rangle$ versus $\ln M$ data. While fitting a straight line we did not take into account the points falling in the saturation region. From the knowledge of $\tau(q)$ one can now establish a connection between intermittency and multifractality, can evaluate the fractal dimensions, and can also construct the most

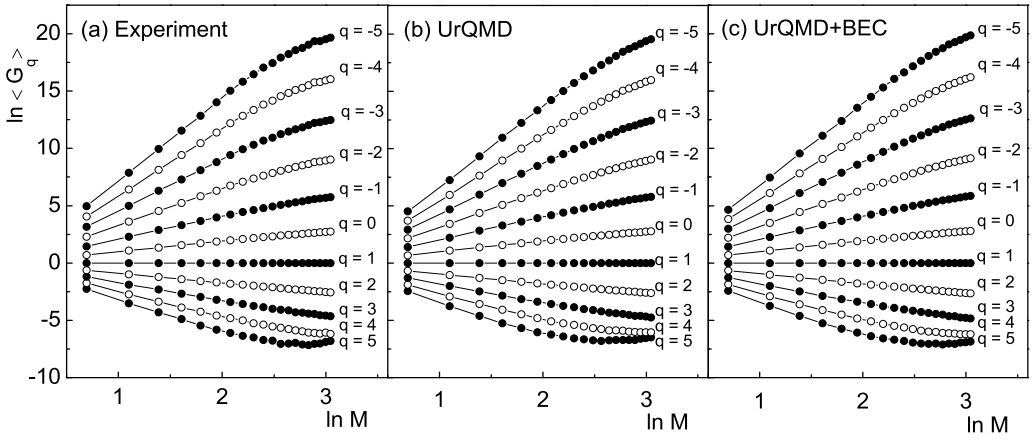

Figure 5.1: Multifractal G_q moment plotted with phase space partition number in ^{28}Si-Ag/Br interaction at 14.5A GeV. Lines joining points are drawn to guide the eye.

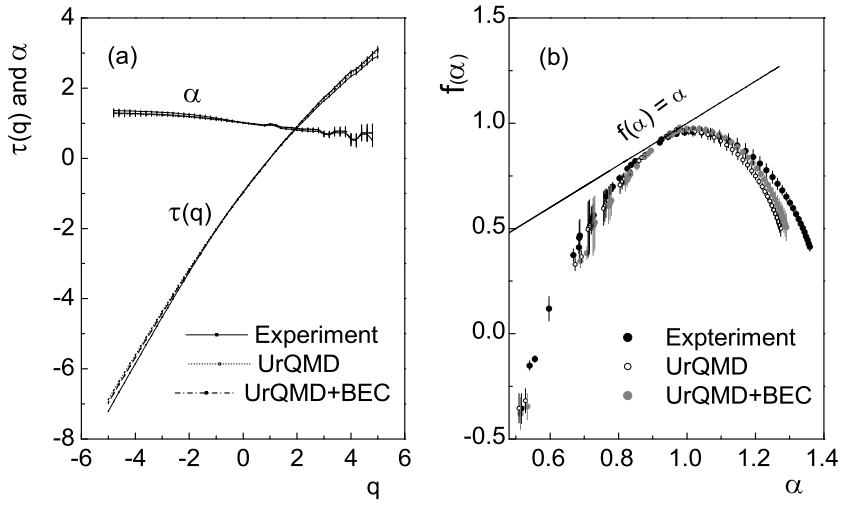

Figure 5.2: (a) The event average mass exponent $\tau(q)$ and the Lipschitz-Hölder exponent α plotted against q. Note that the experiment (solid line), the UrQMD (dotted line) and the UrQMD+BEC (dashed line) are very close to each other. (b) The multifractal spectral function for the experiment (solid circles), the UrQMD (open circles) and the UrQMD+BEC (shaded circles).

important multifractal singularity spectral function [23],

$$f(\alpha) = q\,\alpha(q) - \tau(q). \tag{5.5}$$

Here the Lipschitz-Hölder exponent α is defined as $\alpha(q) = \partial\tau(q)/\partial q$. The importance of the singularity spectrum in the theory of multifractals is that, the width of the spectrum is a direct measure of the degree of multifractality present in the data, which for a monofractal object should reduce to a delta function centered around a particular $\alpha(q) = \alpha(0)$. A finite width of $f(\alpha)$ distribution on the other hand would suggest that, the quantitative nature of the singularities of particle density, as the scaling law (5.1) suggests, may be different at different phase space points, and not guided by any universal exponent. In Fig. 5.2(a) we have shown a plot of $\tau(q)$ against q for the experiment and the simulations. Corresponding α values are also presented in the same diagram. One can notice that the experimental and the simulated results behave almost identically. It can also be seen that (i) there exists a small but definite non-linearity in the variation of $\tau(q)$ with q, and (ii) a decreasing trend of α with increasing q. In the phenomenology of multifractality both the observations indicate the presence of multifractality in the actual density distribution [5, 6]. The multifractal spectral functions $f(\alpha)$, obtained for the experiment, for the UrQMD simulation with and without BEC are plotted in Fig. 5.2(b). All the spectra are found to be very stable, smooth and concave downwards having peaks at $\alpha(q = 0)$. The straight line $f(\alpha) = \alpha$ shown in the diagram, tangentially touches all the spectra at around $\alpha \approx 1.0$. The maxima of $f(\alpha)$ is very close to unity, indicating that the empty bin effect, especially within the scale region of analysis, has properly been taken care of. A wide $f(\alpha)$ spectrum for all the data

samples is strengthening the proposition of multifractality. The important issue is that the experimental spectrum is wider than both the UrQMD and UrQMD+BEC generated spectra, and the UrQMD+BEC spectrum falls in between the experimental and the UrQMD generated spectra. This is an indication of the fact that multifractality in the experimental data is greater than the UrQMD simulation, and inclusion of BEC actually enhances the multifractal character of the UrQMD data. Similar effect has also been observed in our intermittency analysis as well [21]. The spectral functions obtained in our analysis exhibit similar features that are observed in the $p\overline{p}$ collisions of the UA1 collaboration [12], or in the AB collisions of the EMU01 [15] experiments. It is to be noted that the UA1 results were compared with the GENCL and the PYTHIA(v4.8) predictions, whereas a stochastic model was used to compare the EMU01 results. As mentioned, in addition to the dynamical component of fluctuation (if any), the G_q moment calculated through Eq. (5.2) is contaminated by the statistical noise. While the dynamical component in the particle density fluctuation can automatically be filtered in the intermittency technique, the same is not true for multifractality. Therefore, it would be a useful exercise to estimate the nontrivial dynamical component of the G_q moment, and to see whether it can match the same obtained from our intermittency analysis. In order to find out the statistical contribution, we have calculated the G_q moments over an uncorrelated event sample (call it $G_q^{\rm sta}$) generated by (pseudo)random numbers as discussed in Chapter 2. For each q corresponding mass exponents $\tau^{\rm sta}(q)$ are also calculated from the best fitted straight lines to the data points. It has been shown in ref. [6] that the dynamical component of $\tau(q)$, denoted by $\tau^{\rm dyn}(q)$ is related to the statistical one $\tau^{\rm sta}(q)$ by the following relation,

$$\tau^{\rm dyn}(q) = \tau(q) - \tau^{\rm sta}(q) + q - 1. \tag{5.6}$$

In deriving the above relation, it has been assumed that $G_q^{\rm dyn}$ obeys the same scaling-law as G_q i.e., $\left\langle G_q^{\rm dyn} \right\rangle \propto (\delta X_\eta)^{\tau^{\rm dyn}(q)}$ as $\delta X_\eta \to 0$. It then follows from Eq. (5.6) that for a trivial dynamics $\tau^{\rm dyn}(q)$ should be equal to $(q-1)$. Therefore, any deviation in $\tau^{\rm dyn}(q)$ from $(q-1)$ may be considered as an outcome of the nontrivial dynamics. A phenomenological relation between the intermittency exponent ϕ_q and the dynamical component of mass exponent $\tau^{\rm dyn}(q)$ after Hwa [6] is given by,

$$\tau^{\rm dyn}(q) - q + 1 \approx \phi_q. \tag{5.7}$$

The effect of eliminating the statistical contribution to the G_q moments can be readily seen from Fig. 5.3, where the $q - 1 - \tau(q)$, the $q - 1 - \tau^{\rm dyn}(q)$, along with the ϕ_q values taken from ref. [21] are plotted together against q. The results obtained from the experiment, the UrQMD and UrQMD+BEC simulation are shown separately to avoid mutual overlapping of the points. Both in the experiment and in the simulations (with and without BEC) the

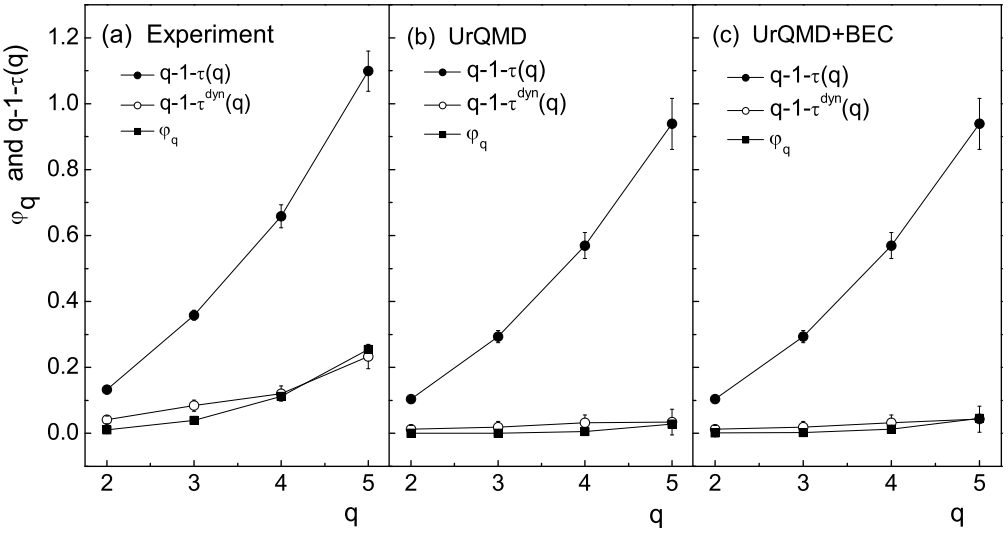

Figure 5.3: Plots of $q-1-\tau^{\rm dyn}(q)$, $q-1-\tau(q)$ and the intermittency exponent ϕ_q [21] versus order number q. In all diagrams lines joining points are drawn to guide the eye.

$q-1-\tau(q)$ values are far above the corresponding ϕ_q values. As soon as the statistical contribution is subtracted, the respective $q-1-\tau^{\rm dyn}(q)$ values come down very close to the intermittency index. It is to be noted that, very little evidence of dynamical fluctuation has been observed in the intermittency analysis ($\phi_q \approx 0$) of the UrQMD data [21, 22], and the UrQMD+BEC estimation of ϕ_q is about $5-10$ times larger than the respective UrQMD values. The UrQMD and the UrQMD+BEC predictions of $q-1-\tau^{\rm dyn}(q)$ also match their respective ϕ_q values. In spite of the fact that the model produces only statistical fluctuations, the UrQMD shows multifractality and the Bose-Einstein correlation included by the prescribed afterburner technique enhances the degree of multifractality. Since the multifractal character is also found in the random number generated sample, the scaling behavior of G_q cannot be taken as the characteristic of the dynamical fluctuation, rather the dynamical signature of the data has to be scrutinized at the level of scaling exponents and derivatives obtained thereof.

A fractal system can also be characterized by a parameter called the Lévy stable index (μ) which has a stability range, $0 \leqslant \mu \leqslant 2$ [24, 25], though occasionally the index is found outside the specified stability range [26]. The upper limit $\mu = 2$ corresponds to minimum fluctuation for a self-similar branching process, whereas the lower limit $\mu = 0$ corresponds to maximum fluctuation i.e., monofractals that may be a signal of a second order phase transition. For the α-model [27], where the final state particle density is given as a product of random numbers, the density function can be approximated by a log-Lévy type of distribution. Under this approximation the Lévy index μ can be determined using the following relation [25, 28]:

$$\frac{D_T - D_q}{D_T - D_2} = \frac{1}{q-1}\frac{q^\mu - q}{2^\mu - 2}, \tag{5.8}$$

where D_T is the topological dimension of the supporting space, which is 1 in the present case, and D_q is the generalized Renyi dimension of integer order q defined in terms of the intermittency exponents ϕ_q as,

$$D_q = D_T - \frac{\phi_q}{q-1}. \tag{5.9}$$

Following Eq. (5.7) one can also set

$$D_q \approx \frac{\tau^{\rm dyn}(q)}{q-1}. \tag{5.10}$$

We shall discuss more about D_q in the next section. In practice only a few D_q values are obtained from the intermittency and/or multifractal analysis. Therefore, the μ value extracted by fitting Eq. (5.8) to a small set of data points is likely to be unreliable. Hence we follow an alternative method of calculating μ using the multifractal spectral function $f(\alpha)$, as described by Hu *et al.* [29]. According to [29], $f(\alpha)$ is related to μ by the following relation,

$$1 - f(\alpha) \propto (B-\alpha)^{\mu/(\mu-1)} \quad \text{for } \alpha < B, \tag{5.11}$$

where with $B = 1 + (1-D_2)/(2^\mu - 2)$. Note that for any q, positive or negative, $f(\alpha)$ is a smooth and continuous function of $\alpha(q)$. Therefore, the index μ can be extracted from the slope $\mathcal{C} = \mu/\mu - 1$ of the $\ln(1-f(\alpha))$ versus $\ln(B-\alpha)$ straight line in the $\alpha < B$ region. As it follows from Eq. (5.11), the only criterion that has to be satisfied here is $f(B) = 1$. Fig. 5.4 shows the results of such calculations. In either of these plots, it is clear that a single straight line cannot reproduce the data well and hence the μ value is found to depend on the region of fitting the straight lines. The best fitted straight lines in two different q-regions are shown in the diagrams. In the positive and low-q region the straight line fit is

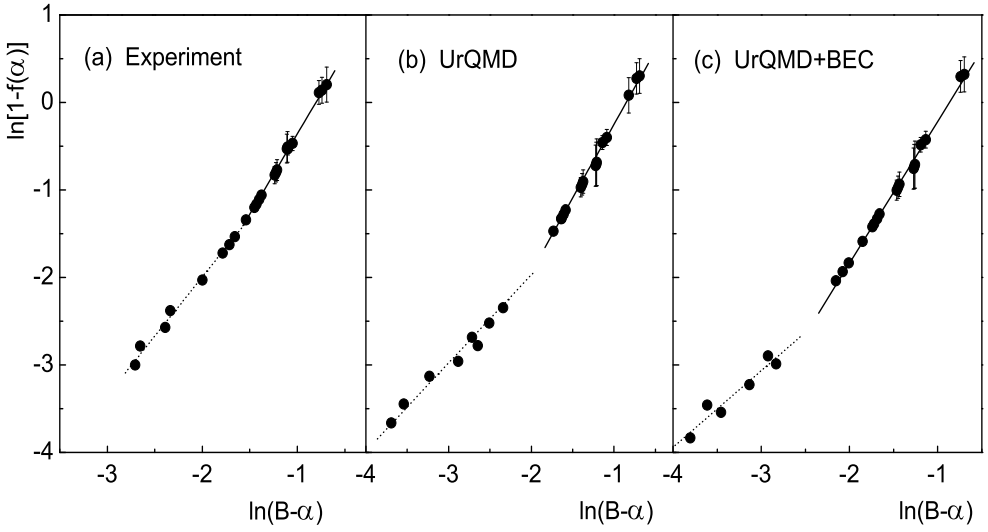

Figure 5.4: Plot of $\ln[B-\alpha]$ versus $\ln[1-f(\alpha)]$. In all diagrams the dotted(solid) lines represent linear fits to the data points in the low(high)-q region.

shown by the dotted line and the solid line represents the linear fit in the positive and high-q region. The values of μ obtained from these fittings are listed in Table 5.1. The experiment and the UrQMD simulation provide somewhat reasonable values of μ in the high-q region, otherwise the index is either diverging or far from the admissible limits. Therefore, one may conclude that the (dynamical) density fluctuations present in our data are not compatible to the log-Lévy type of distributions.

Table 5.1: The values of the Lévy stable index (μ) obtained at two different regions of q in ^{28}Si-Ag/Br interaction at 14.5A GeV.

Fit region	Experiment	UrQMD	UrQMD+BEC
Low-q region	3.843±0.089	$\to \infty$	6.880±0.0.0124
High-q region	2.199±0.164	2.466±0.152	-2.6129±0.0801

5.3 Takagi's Moment

In order to study the multifractal structure of particle density distributions, Takagi proposed a new set of moments called the T_q moments [7]. Takagi's method is based on two assumptions: (i) the density distribution ρ is uniform all over the phase space interval and (ii) the multiplicity distribution P_n does not depend on the location of the phase space interval. Both these criteria are found to be more or less valid when the cumulative variables are used in place of the basic phase space variable like η or φ. The T_q moment for positive integer order q is defined as,

$$T_q(\delta X_\eta) = \ln \sum_{i=1}^{N_{ev}} \sum_{j=1}^{M} (p_{ij})^q, \tag{5.12}$$

where $p_{ij} = n_{ij}/K$, K being the total number of tracks present in all N_{ev} events, and n_{ij} is the number of tracks in the jth bin of the ith event. Unlike the G_q moments, the T_q moments so defined are not very much affected by the finiteness of an event multiplicity $\langle n_s \rangle$. According to Takagi [7], $T_q(\delta X_\eta)$ should be a linear function of $\ln(\delta X_\eta)$, i.e.

$$T_q(\delta X_\eta) = A_q + B_q \ln(\delta X_\eta), \tag{5.13}$$

where A_q and B_q are two constants independent of the phase space resolution size. When a linear relation like Eq. (5.13) is observed over a considerable range of δX_η, the generalized

dimension D_q can be obtained in terms of the fit parameter B_q as

$$D_q = \frac{B_q}{q-1}, \quad \text{for } q \geqslant 2. \tag{5.14}$$

For a sufficiently large N_{ev} one can set

$$\sum_{i=1}^{N_{ev}} \sum_{j=1}^{M} (p_{ij})^q = \frac{\langle n^q \rangle}{K^{q-1} \langle n \rangle}, \tag{5.15}$$

where $\langle n \rangle$ represents the average bin multiplicity. From Eq. (5.12)–(5.15) and replacing δX_η by $\langle n \rangle$ one can derive an expression for the generalized dimension for $q \geqslant 2$ through the following relation:

$$\ln \langle n^q \rangle = A_q + \{(q-1)D_q + 1\} \ln \langle n \rangle . \tag{5.16}$$

For $q = 1$ the parameter D_1 is known as the information dimension, which provides the information of how much of a phase space interval is filled up with the distributed tracks. D_1 is obtained by taking an appropriate limit to Eq. (5.14) [30]. This is equivalent to considering an entropy like function

$$\mathcal{S}(\delta X_\eta) = -\sum_{i=1}^{N_{ev}} \sum_{j=1}^{M} p_{ij} \ln p_{ij}, \tag{5.17}$$

and to looking for its linear dependence on $\ln(\delta X_\eta)$,

$$\mathcal{S}(\delta X_\eta) = -D_1 \ln(\delta X_\eta) + \text{constant}. \tag{5.18}$$

Using Eq. (5.15) one can now easily obtain an expression for D_1 as,

$$\langle n \ln n \rangle / \langle n \rangle = C_1 + D_1 \ln \langle n \rangle . \tag{5.19}$$

Following the prescription of Takagi [7], we have calculated $\langle n \ln n \rangle$ and $\ln \langle n^q \rangle$ (for $q = 1 - 7$) with increasing phase space interval δX_η taken symmetrically about the centroid of the η-distribution. The results are shown graphically in Fig. 5.5 for all the data sets employed in this analysis. The information dimension D_1 is evaluated from the best fitted straight lines to the $\langle n \ln n \rangle / \langle n \rangle$ versus $\ln \langle n \rangle$ plot and is shown in the upper panel of the Fig. 5.5. The generalized dimensions D_q are evaluated from the best linear fits to the $\ln \langle n^q \rangle$ versus $\ln \langle n \rangle$ graph for $q = 2 - 7$. It turns out that $D_1 = 0.933 \pm 0.037$ for the experiment, $D_1 = 0.926 \pm 0.005$ for the UrQMD, $D_1 = 0.935 \pm 0.005$ for the UrQMD+BEC and $D_1 = 0.934 \pm 0.005$ for the random number generated event sample. All these values are slightly less than the phase space dimension, which according to the theory of fractals, is a signature of fractal density distribution function. The generalized dimensions D_q obtained

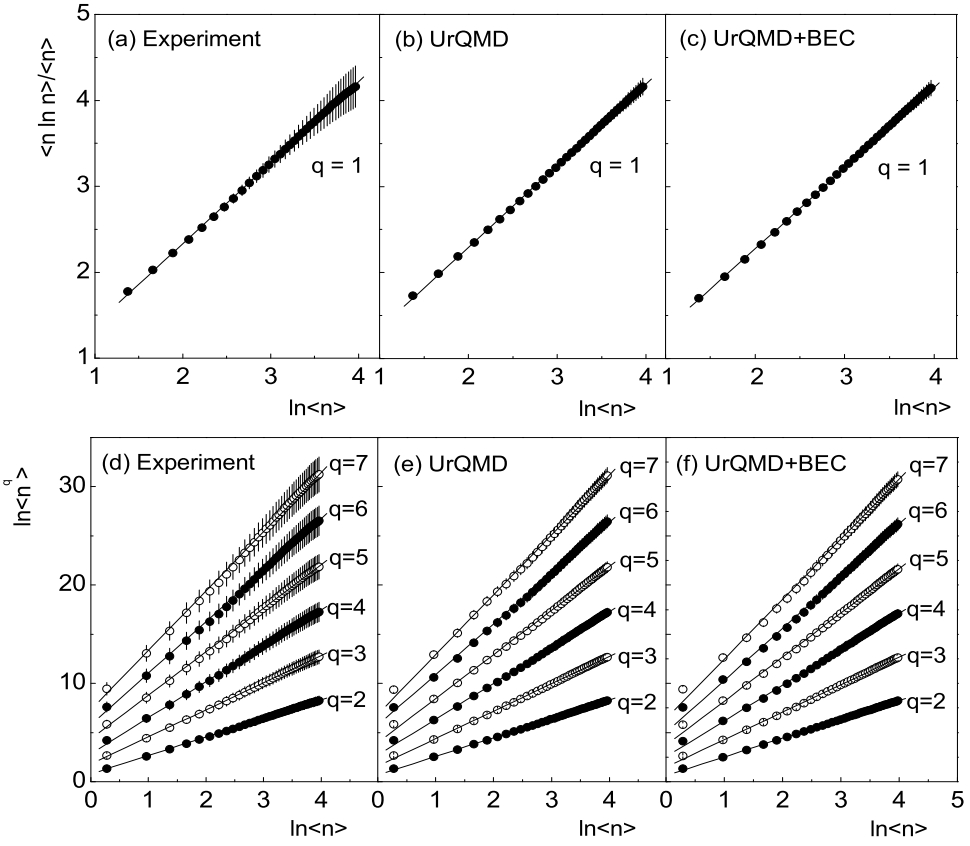

Figure 5.5: Multifractal T_q moment as a function of number of counts in the phase space interval. The best fitted straight lines are shown in all diagrams.

from Takagi's moments [Eq. (5.16)], and those obtained from Hwa's moments [Eq. (5.10)] are plotted together against q in Fig. 5.6. On the same figure we have included the D_q values obtained from the SFM analysis [21]. A general decreasing trend of D_q with increasing q has been observed for all three data samples, which again indicates multifractality. In the case of experiment the D_q values obtained from the SFM fall at a much faster rate than those obtained from the G_q moment, whereas for UrQMD the D_q values calculated either form the SFM or from the G_q moment, within the errors are very close to unity, which is the dimension of the supporting space. The UrQMD+BEC data, on the other hand, shows a rapid fall in D_q when calculated from the SFM but the rate of fall is not as high as the experimental one. The D_q values obtained from the T_q moment for all the data sets are significantly and consistently lower than those obtained from the SFMs and the G_q moments. Such a large and systematic deviation might reflect the fact that the T_q moments are not corrected from the statistical contamination, the technique of which is still unknown to us. Moreover, the moments are defined in different ways, which might be another source of such inconsistencies. Note that for a simple Poissonian type of multiplicity distribution within a given interval δX_η, the generalized dimensions would all be equal to the topological dimension of the supporting space. Any deviation from unity, as it is observed in

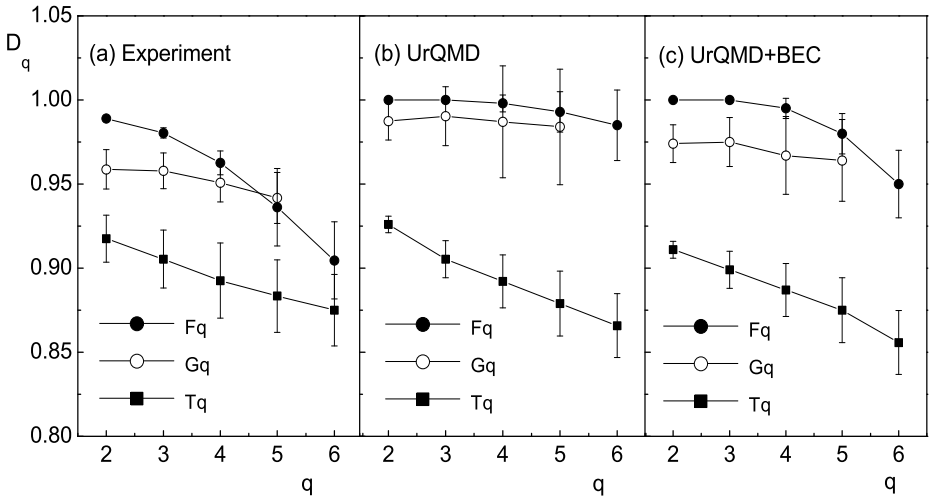

Figure 5.6: Generalized dimensions D_q with order number q calculated from the SFM (solid circles) [21], G_q moment (open circles) and T_q moment (solid square) analysis. The lines joining points are shown to guide the eye.

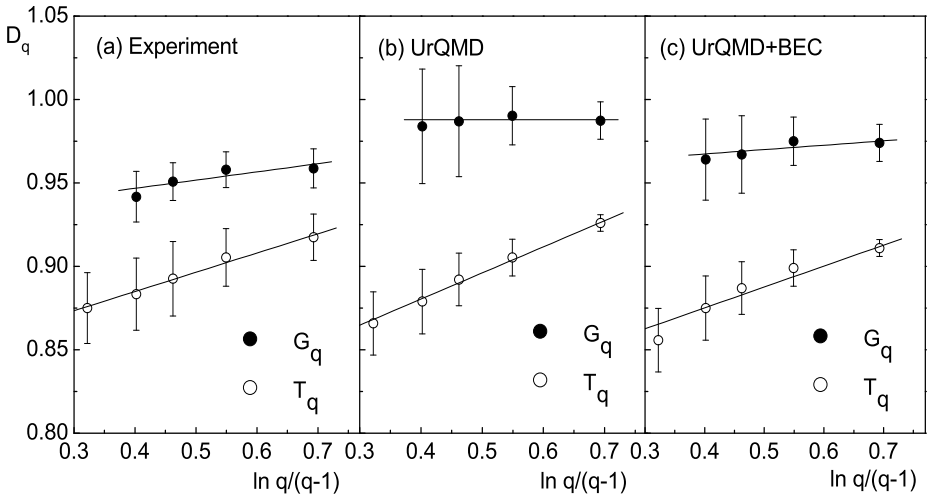

Figure 5.7: Plot of D_q with $\ln q/(q-1)$. The solid (open) circles are the results of the $G_q(T_q)$ moment analysis. The lines are the best linear fits to the data points.

our analysis, should therefore be considered as a signature of nonstatistical elements present in the particle distribution.

The thermodynamic interpretation of fractals in terms of the multifractal specific heat, has been given by Bershadski [31]. If the monofractal to the multifractal transition is governed by a Bernoulli type of fluctuation only, then the multifractal specific heat C can be derived from the relation [31]:

$$D_q = D_\infty + \frac{C \ln q}{q-1}. \tag{5.20}$$

A monofractal to multifractal transition corresponds to a jump from $C = 0$ to a nonzero

finite value. In Fig. 5.7 we have plotted D_q against $\ln q/(q-1)$ for (a) the experiment, (b) the UrQMD and (c) the UrQMD+BEC data, and the values obtained from both Hwa's moments and Takagi's moments are shown together. An approximately linear dependence of D_q on $\ln q/(q-1)$ is observed for all three data samples, indicating the relevance of Bershadski's interpretation of multifractality [31] in the context of a phase transition in the present case. The C values are extracted from the best linear fits to the data points shown in the diagrams. The values of C are quoted in Table 5.2. The effect of eliminating the statistical noise using the random number generated event sample is manifested once again in the C value obtained from Hwa's method, which produces almost null value of C for the simulated events. On the other hand, in Takagi's method no distinction is possible between the experiment and the UrQMD predictions, but for some reason that cannot be clarified at this point, inclusion of BEC lowers the value of C by about ten times the experiment/UrQMD prediction. The present set of C values are not consistent with the universality as it was claimed in ref. [31].

Table 5.2: The values of multifractal specific heat C calculated from the G_q and T_q moment analysis of the ^{28}Si-Ag/Br data at 14.5A GeV.

Method employed	Experiment	UrQMD	UrQMD+BEC
Hwa's moments	0.0493±0.0076	0.00004±0.09055	0.0261±0.0074
Takagi's moments	0.1154±0.0598	0.1566±0.0371	0.0125±0.0371

5.4 Multifractal Detrended Fluctuation Analysis

The details of the multifractal detrended fluctuation analysis (MF-DFA) method is given in ref. [8], however for the sake of completeness we provide a brief description of this method in the following section.

Let $\{x_k : k = 1,\ 2, \ldots, N\}$ be a fluctuating signal of length N. In our case x_k is nothing but the single particle η-density values in an event. The MF-DFA procedure consists of the following steps:

(i) Determine a profile series through

$$Y(i) = \sum_{k=1}^{i} [x_k - \langle x \rangle], \quad i = 1,\ 2, \ldots, N, \tag{5.21}$$

where $\langle x \rangle = (1/N) \sum_{i=1}^{N} x_i$ is the mean value of the signal to be analyzed.

(ii) Divide the profile $Y(i)$ into $N_M = int(N/M)$ non-overlapping segments of equal length M. One has to choose the M value depending upon the signal length. If the length N is not a multiple of the considered scale M, then the same dividing procedure is repeated starting from the opposite end of the series. Hence, in order not to disregard any part of the signal, usually altogether $2N_M$ segments of equal length are obtained.

(iii) Calculate the local trend for each of the $2N_M$ segments. This is done by least-square fits of the segments (or subseries). Linear, quadratic, cubic or even a higher order polynomial may be used to detrend the series, and accordingly the procedure is said to be the MF-DFA1, MF-DFA2, MF-DFA3, $\cdots$ analysis. Here we use a linear fit, and hence the detrended method is denoted as MF-DFA1. Let, y_ν be the best fitted polynomial to an arbitrary segment ν of the signal. Then determine the variance

$$F^2(\nu, M) = \frac{1}{M}\sum_{i=1}^{M}\{Y[(\nu-1)M+i] - y_\nu(i)\}^2 \tag{5.22}$$

for $\nu = 1, \cdots, N_M$, and the same for $\nu = N_M+1, \cdots, 2N_M$ is given as

$$F^2(\nu, M) = \frac{1}{M}\sum_{i=1}^{M}\{Y[N-(\nu-N_M)M+i] - y_\nu(i)\}^2 . \tag{5.23}$$

(iv) The MF-DFA fluctuation function (moment) F_q is defined by averaging the variance $F^2(\nu, M)$ over all the $2N_M$ segments as,

$$F_q(M) = \left\{\frac{1}{2N_M}\sum_{\nu=1}^{2N_M}[F^2(\nu, M)]^{q/2}\right\}^{1/q} \quad \forall\ q \neq 0, \tag{5.24a}$$

$$F_q(M) = \exp\left\{\frac{1}{4N_M}\sum_{\nu=1}^{2N_M}\ln[F^2(\nu, M)]\right\} \quad \text{for } q = 0. \tag{5.24b}$$

In general, the order parameter q can take any real value.

(v) Finally varying the scale parameter M, i.e. the phase space partition number, one can study the scaling behavior of the detrended fluctuation functions.

If the series $\{x_k\}$ possesses long-range correlation, $F_q(M)$ for large values of M would follow a power-law type of scaling relation, such as

$$F_q(M)|_{M\to\infty} \propto M^{h(q)} \quad \forall\ q. \tag{5.25}$$

The exponent $h(q)$, in general a function of q, is said to be the generalized Hurst exponent [8]. It follows that $h(2) = H$, the well known Hurst exponent. The series $\{x_k\}$ is considered

as long-range anti-correlated if $0 < H < 0.5$, uncorrelated if $H = 0.5$ and long-range correlated if $H > 0.5$. Although such a classification is based on the consideration that the signal $\{x_i\}$ is a stationary one, such as the fractional Gaussian noise (fGn) [32]. For non-stationary signals e.g., the fractional Brownian motion (fBm), H is related to $h(2)$ through $H = h(2) - 1$ and $h(2) > 1.0$ [33]. For a monofractal series $h(q)$ is independent of q since the variance $F^2(\nu, M)$ is identical for all the subseries, and hence Eq. (5.24) yields identical values for all q. Note that the function F_q can be defined only for $M \geqslant m + 2$, where m is the order of the detrending polynomial. Moreover, F_q is statistically unstable for very large M ($\geqslant N/4$). If small and large fluctuations scale differently, there will be a significant dependence of $h(q)$ on q. Whereas for positive values of q, F_q will be dominated by the large variance which corresponds to the large deviations from the detrending polynomial, for negative values of q major contributions of F_q arise form small fluctuations from the detrending polynomial. Thus, for positive (negative) values of q, $h(q)$ describes the scaling behavior of the segment with large (small) fluctuations. Note that the MF-DFA method is a kind of generalization of the detrended fluctuation analysis (DFA) [33], introduced to study the scaling properties of DNA sequences [33, 34]. For $q = 2$ the function defined in Eq. (5.24)(a) reduces to the ordinary DFA fluctuation function.

5.4.1 Relation with Standard Multifractal Variables

One can easily relate the $h(q)$ exponent with the standard multifractal exponent, such as the multifractal (mass) exponent $\tau(q)$. Suppose the series $\{x_k\}$ is stationary and normalized. Then the detrending procedure in step (iii) of the above methodology is not required. The variance of such a series is given by

$$F_N^2(\nu, M) = \{Y(\nu M) - Y[(\nu - 1)M]\}^2, \tag{5.26}$$

and the fluctuation function and its scaling-law would be

$$F_q(M) = \left\{ \frac{1}{2N_M} \sum_{\nu=1}^{2N_M} |Y(\nu M) - Y[(\nu - 1)M]|^q \right\}^{1/q} \sim M^{h(q)}, \quad \forall\ q. \tag{5.27}$$

Now if we assume that the length of the series N is an integer multiple of the partition number M, then the above relation can be rewritten as

$$\sum_{\nu=1}^{N/M} |Y(\nu M) - Y[(\nu - 1)M]|^q \sim M^{qh(q)-1}. \tag{5.28}$$

In the above relation the term under $|\cdot|$ is nothing but the sum of $\{x_k\}$ within an arbitrary νth segment of length M. In the standard theory of multifractals it is known as the box probability $p(M,\nu)$ for the series $\{x_k\}$. Hence,

$$p(M,\nu) \equiv \sum_{k=(\nu-1)M+1}^{\nu M} x_k = Y(\nu M) - Y((\nu-1)M). \tag{5.29}$$

The multifractal scaling exponent $\tau(q)$ is defined through the partition function $Z_p(M)$ as

$$Z_p(M) \equiv \sum_{\nu=1}^{N/M} |p(M,\nu)|^q \sim M^{\tau(q)}, \tag{5.30}$$

where q is a real parameter. From Eq. (5.28) to Eq. (5.30) it is clear that the multifractal exponent $\tau(q)$ is related to $h(q)$ through the following relation

$$\tau(q) = q\,h(q) - 1. \tag{5.31}$$

After knowing $\tau(q)$ once again we can calculate the multifractal singularity spectrum: $f(\alpha) = q\,\alpha - \tau(q)$ and the generalized fractal dimension $D_q = \tau(q)/(q-1)$. Here $\alpha = \partial\tau/\partial q$ is the Lipschitz-Hölder exponent also known as the singularity strength parameter [23].

5.4.2 Results of Multifractal Detrended Fluctuation Analysis

As mentioned, the detrended method has been originally developed for the (multi)fractal characterization of the time series data of effectively infinite length. Here we apply the methods to the single event η distributions of particles produced in ^{28}Si-Ag/Br collision at 14.5A GeV. In our event sample the event-to-event multiplicity varies over a wide range, and there exists a large number of low multiplicity events where the detrended technique cannot be applied. Therefore, we impose a shower multiplicity cut of $n_s > 50$ that makes the average shower multiplicity $\langle n_s \rangle \sim 80$. Further, we have as many signals as the number of events present in the sample. Therefore we take an average of the single event MF-DMA fluctuation function $F_q^{(e)}$ over the event sample. In this way we actually study the average behavior of the detrended fluctuation functions i.e., $\langle F_q \rangle = (1/N_{ev}) \sum F_q^{(e)}$, and the scaling relation (5.25) reads as

$$\langle F_q \rangle|_{M\to\infty} \propto M^{h(q)} \quad \forall\ q. \tag{5.32}$$

Accordingly, the exponent $h(q)$ and other multifractal variables derived thereof are none other than their event space averaged values. We show the event averaged DFA fluctuation functions $\langle F \rangle = \langle F_{q=2} \rangle$ with phase space partition number M in Fig. 5.8 for (a) the experiment, (b) the UrQMD and (c) the UrQMD+BEC. In this analysis we vary M from

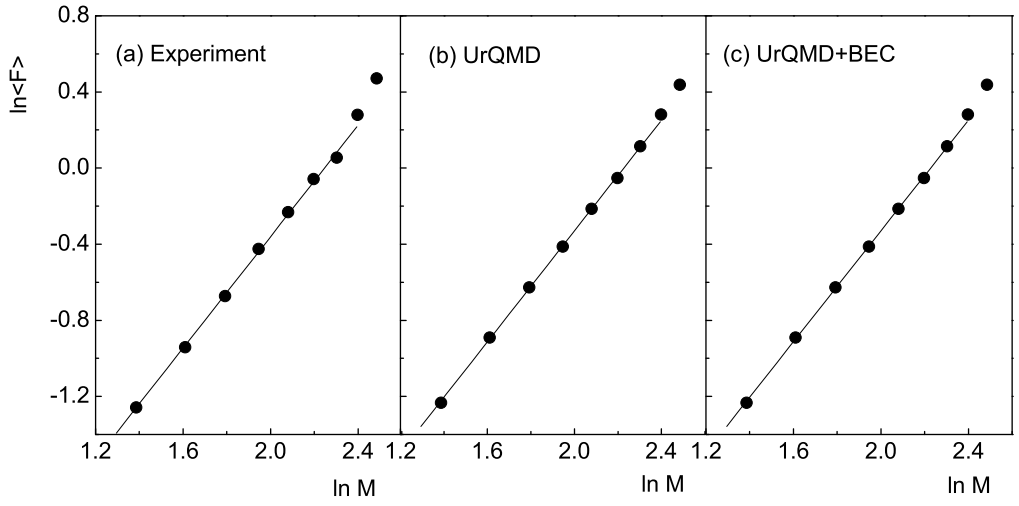

Figure 5.8: Event averaged DFA fluctuation functions $\langle F_{q=2} \rangle$ plotted with phase space partition number. The lines represent the best linear fits to the data points in the linear region.

Table 5.3: The values of the Hurst exponent H and the fractal dimension D_F calculated from the MF-DFA method for the ^{28}Si-Ag/Br interaction data at 14.5A GeV.

Parameter	Experiment	UrQMD	UrQMD+BEC	Random
H	1.463±0.021	1.456±0.019	1.450±0.018	1.446±0.017
D_F	0.537±0.021	0.544±0.019	0.550±0.018	0.554±0.017

4 to $n_s^{\min}/4$, where $n_s^{\min}$ is the least multiplicity of the event sample (here $n_s \geqslant 50$). It is noticed that the data points are nicely reproduced by the scaling-law (5.32). The Hurst exponent H is evaluated from a straight line fit to the $\ln \langle F \rangle$ versus $\ln M$ data points in the region $4 \leqslant M \leqslant 10$, since a couple of points at large-M side slightly deviate from the initial linear trend. The H values are given in Table 5.3 for all the data sets. We repeat the analysis for a random number generated event sample, and the corresponding value of H is also put in the table. As mentioned earlier, the exponent H allows us to identify the type of correlation present in the signals. Accordingly, we argue that a long-range correlation may exist in all the cases studied. The values of fractal dimension (D_F) calculated from the H values are given in the same table. We know that for a fractal object $D_F < D_T$, the topological dimension of the supporting space (here unity), and the deviation of D_F from D_T is a measure of the degree of fractality. The results of the DFA analysis therefore, demand that the η-distribution for the ^{28}Si-Ag/Br interaction is highly fractal in nature.

We compute the event averaged MF-DFA1 fluctuation function $\langle F_q \rangle$ for $q = -5$ to 5 with an incremental step of 0.25. Some of them (for integer q only) are plotted against M in Fig. 5.9 for the experiment, UrQMD and UrQMD+BEC samples. Apparently we do not

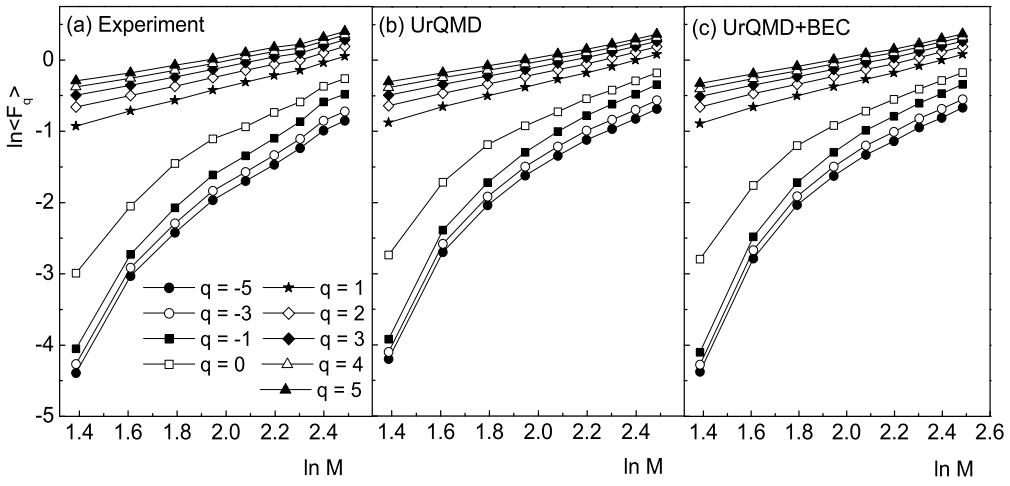

Figure 5.9: Event averaged MF-DFA1 fluctuation functions plotted with phase space partition number for integer $q \in [-5, +5]$ in ^{28}Si-Ag/Br interaction at 14.5A GeV. Lines joining points are drawn to guide the eye.

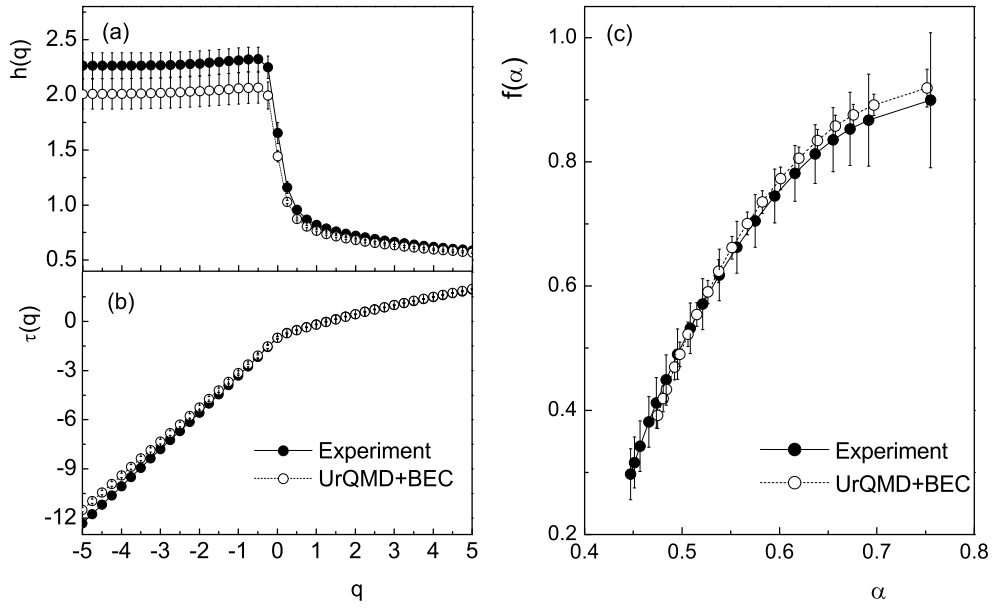

Figure 5.10: (a) Plot of $h(q)$ versus q, (b) $\tau(q)$ versus q, and (c) the singularity spectra $f(\alpha)$ obtained from the MF-DFA1 method. Lines joining points are shown.

find any difference between the experimental and the model simulated values of F_q. The scaling behavior of the $\langle F_q \rangle$-functions are not linear over the entire scale range, especially for the $F_{q\leqslant 0}$ functions which are nonlinear in the low-M region. Therefore we compute $h(q)$ in the large-M region ($6 \leqslant M \leqslant 12$), where the scaling relation (5.25) holds satisfactorily. This is not a surprising phenomenon and the reason of which is already mentioned and also specified in Eq. (5.25). It is to be noted that unlike the G_q moments [Section 5.2] the detrended moments of this analysis are not influenced by the finiteness of the event multiplicity. The multifractal parameters, namely (a) the generalized Hurst exponents $h(q)$,

(b) the multifractal mass exponents $\tau(q)$ and (c) the singularity spectra $f(\alpha)$, measured from the MF-DFA1 fluctuation functions are shown in Fig. 5.10. We have dropped the UrQMD generated spectrum from this diagram since it almost coincides with the UrQMD+BEC plot. A number of observations can be made from this figure, which are: (i) $h(q)$ for $q \leqslant -1$ is approximately constant at ~ 2, then it falls rapidly in the $q = -1$ to 1 region and tends to saturate at $h(q) \sim 0.5$ for $q \geqslant 1$, (ii) the $\tau(q)$ spectra are nonlinear, especially in the $q \approx 0$ region, (iii) the singularity spectra are smooth and nonlinear function of α and (iv) the difference between the experiment and UrQMD+BEC (and also UrQMD) simulation is insignificant. Since the $h(q < 0)$ values are approximately constant, all the $f(\alpha)$ values for $q < 0$ are assemble together around a fixed point that results in an unstable singularity spectrum for $q < 0$. A similar observation has also been made for a set of high multiplicity ^{32}S-Ag/Br event sample at 200A GeV [35]. Till date the MF-DFA technique has not been widely used in multiparticle data analysis, and therefore, we are not in a position to make a direct comparison of our results with similar other such analysis. In ref. [18] also the singularity spectrum for $q < 0$ has been found to be unstable. The MF-DFA method D_q values are compared with all the other methods of this analysis in Section 5.5.1.

5.5 Multifractal Detrended Moving Average Analysis

The multifractal detrended moving average (MF-DMA) analysis technique shares many ideas with the detrended fluctuation analysis, but an added advantage in the former method probably makes it more sophisticated over the latter one. The advantage in MF-DMA analysis is that it gives us the freedom to chose the location of the detrending window with respect to the measurement to be detrended. On the other hand, while in MF-DFA one can detrend the signal under consideration by a polynomial of desired order, in MF-DMA the signal has to be detrended only by the average value of the series. The MF-DMA analysis method is nicely described in ref. [9]. In the following subsection a brief outline of the method is itemized below. Like in the MF-DFA case let $\{x_i : \ i = 1, \ 2, \cdots, N\}$ be a fluctuating signal of length N, which in our case is the single particle η-distribution function in an event. The MF-DMA procedure consists of the following steps.

(i) Construct an integrated sequence

$$Y(i) = \sum_{k=1}^{i} [x_k - \langle x \rangle], \quad i = 1, 2, \cdots, N \tag{5.33}$$

with respect to the mean $\langle x \rangle = (1/N) \sum_i x_i$. In the subsequent steps the above sequence is considered as the signal.

(ii) Calculate the moving average function $\widetilde{y}(i)$ in a moving window of size M through

$$\widetilde{Y}(i) = \frac{1}{n} \sum_{k=-\lfloor (M-1)\theta \rfloor}^{\lceil (M-1)(1-\theta) \rceil} Y(i-k), \tag{5.34}$$

where $\lfloor \xi \rfloor$ is the largest integer not larger than ξ and $\lceil \xi \rceil$ is the smallest integer not smaller than ξ. Here θ is a parameter $\in [0,\ 1]$ that specifies the position of the moving window and it is said to be the window parameter. In general the moving average function includes $\lceil (M-1)(1-\theta) \rceil$ data points in the past and $\lfloor (M-1)\theta \rfloor$ data points in the future with respect to the point/variable to be detrended (say x_λ). Here we consider $\theta = 0.5$ for which the moving average function $\widetilde{Y}(i)$ is equally extended on both sides of x_λ, and hence the moving window is said to be the 'central moving' window. Note that for $\theta = 0$ the moving average function $\widetilde{Y}(i)$ is calculated over all the n data points in the past ($x_{k<\lambda}$), while for $\theta = 1$ the function is calculated over all the n data points in the future ($x_{k>\lambda}$), and accordingly the detrending windows are said to be the 'backward moving' and 'forward moving' windows, respectively.

(iii) Detrend the sequence $Y(i)$ by subtracting $\widetilde{Y}(i)$ and obtain the residue series,

$$e(i) = Y(i) - \widetilde{Y}(i), \tag{5.35}$$

where i satisfies the criterion: $M - \lfloor (M-1)\theta \rfloor \leqslant i \leqslant N - \lfloor (M-1)\theta \rfloor$.

(iv) Divide the series $e(i)$ into $N_n = \lfloor N/M - 1 \rfloor$ non-overlapping segments of equal length M. Let the segments are denoted by e_v so that $e_v(i) = e(l+i)$ for $1 \leqslant i \leqslant M$ and $l = (v-1)M$. For an arbitrary segment v the mean-square fluctuation function $\mathcal{F}_v^2(M)$ is calculated as a function of M,

$$\mathcal{F}_v^2(M) = \frac{1}{M} \sum_{i=1}^{M} \{e_v(i)\}^2. \tag{5.36}$$

(v) The overall qth order MF-DMA fluctuation function $\mathcal{F}_q(M)$ is then defined as,

$$\mathcal{F}_q(M) = \left\{ \frac{1}{N_n} \sum_{v=1}^{N_n} [\mathcal{F}_v^2(M)]^{q/2} \right\}^{1/q} \qquad \forall q \neq 0, \tag{5.37a}$$

$$\mathcal{F}_q(M) = \exp\left\{ \frac{1}{2N_n} \sum_{v=1}^{N_n} \ln[\mathcal{F}_v^2(M)] \right\} \text{ for } q = 0. \tag{5.37b}$$

(vi) The scaling behavior of $\mathcal{F}_q(M)$ is examined for a set of q exponents. If the signal $\{x_i\}$ contains multifractality (long-range correlation), $\mathcal{F}_q(M)$ for large values of M would

follow a power-law type of scaling relation, such as

$$\mathcal{F}_q(M)|_{M\to\infty} \propto M^{h(q)}, \tag{5.38}$$

and the exponent $h(q)$ known as the generalized Hurst exponent, would be a nonlinear function of q.

Knowing $h(q)$ once again we can calculate the multifractal scaling exponent $\tau(q)$, the multifractal singularity spectrum $f(\alpha)$, and the generalized multifractal dimensions D_q. The formulae are given in sub-section 5.4.1. Needless to mention that similar to the MF-DFA method here also we study the average behavior of the fluctuation function $\mathcal{F}_q(M)$, and the above scaling-law becomes

$$\langle\mathcal{F}_q\rangle|_{M\to\infty} \propto M^{h(q)}. \tag{5.39}$$

5.5.1 Results of Multifractal Detrended Moving Average Analysis

In Fig. 5.11 the event averaged MF-DMA ($\theta = 0.5$) fluctuation functions $\langle\mathcal{F}_q\rangle$ are plotted for $q = 0, \pm2, \pm5$ versus the phase space partition number M. Actually we have calculated the function $\langle\mathcal{F}_q(M)\rangle$ for all q values between -5 and $+5$ with an incremental step of 0.25, but all of them are not shown in the diagram to maintain clarity. One can see that the scaling behavior of $\langle\mathcal{F}_q(M)\rangle$ is not linear over the entire region, especially not at low M, although the nonlinearity is not as prominent as it is in the case of the MF-DFA functions. Like the MF-DFA methods the MF-DMA method with $\theta = 0.5$ also produces visually identical variation of $\mathcal{F}_q$ in both the simulated samples as the experiment, and therefore, we again drop the UrQMD results from the diagrams of our subsequent MF-DMA analysis. For a given q the exponent $h(q)$ is calculated from the log-log plot of the fluctuation function $\langle\mathcal{F}_q(M)\rangle$ in the large-M region. Here we take $8 \leqslant M \leqslant 18$, since the best linear behavior of the functions $\langle\mathcal{F}_q(M)\rangle$ is found in this region. The $h(q)$ values so obtained are plotted against q in Fig. 5.12(a), while the corresponding multifractal exponents $\tau(q) = qh(q) - 1$ are plotted in Fig. 5.12(b). It is seen that in the experiment the q dependence of both $h(q)$ and $\tau(q)$ values are stronger than the UrQMD+BEC (and also the UrQMD) generated values. Unlike the $h(q) - q$ plot of the MF-DFA method [see Fig. 5.10], here we obtain a smoothly varying $h(q)$ values for the experiment as well as for the simulations. The existence of a multifractal pattern in the particle density function can be conjectured for all the data samples studied. The calculated $h(q = 2)$ values are 0.619 ± 0.047 (Experiment) and 0.878 ± 0.039 (UrQMD+BEC). The parameter $h(2)$ indicates that the η-distributions are similar to the stationary time series signal for which $h(2) = H$, the ordinary Hurst exponent, and that the η-distribution functions have long-range correlation ($H > 0.5$). In

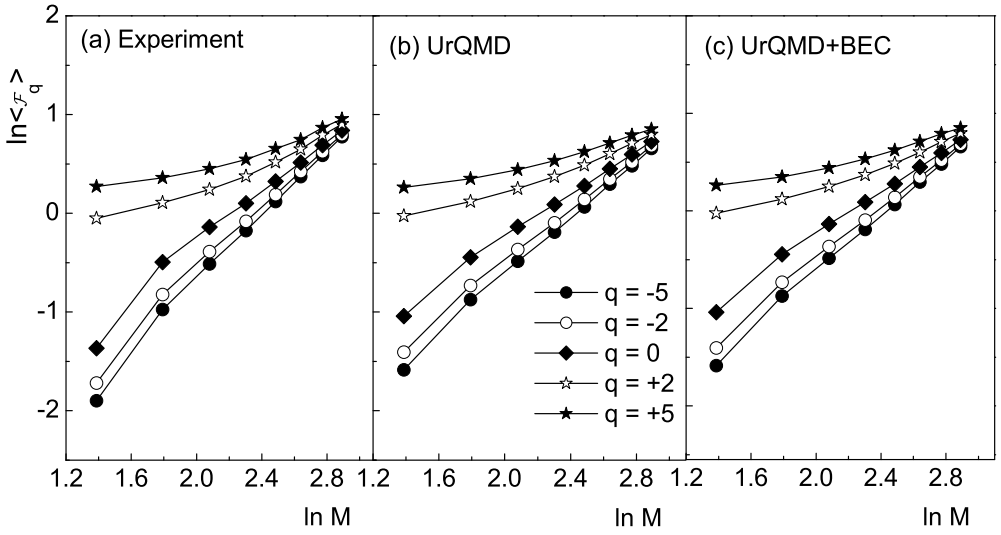

Figure 5.11: Event averaged MF-DMA ($\theta = 0.5$) fluctuation functions for the window parameter $\theta = 0.5$. Lines joining points are drawn to guide the eye.

diagram 5.12(c) we present the singularity spectra obtained from the MF-DMA technique. The $f(\alpha)$ spectra have a similar look as those obtained from the G_q moment analysis for the same set of data, but without any multiplicity cut as imposed in the detrended analysis. It is worth mentioning that the $f(\alpha)$ spectra of the MF-DFA technique are found to be unstable for $q < 0$. In contrast, the singularity spectra obtained in this method are smooth and bell-shaped functions of the Lipschitz-Hölder exponent α. A mismatch between the experiment and the UrQMD+BEC simulation, mainly at the low-α side of the spectra, is prominent. The difference originates from a mismatch between the corresponding $h(q)$ values. Another important observation of the diagram is that, the experimental spectrum is slightly right-skewed (skewness ≈ 0.052). Such an asymmetric $f(\alpha)$ spectrum implies that the pronounced multifractality appears from a small scale (noise like) fluctuation, while the dynamics of large scale fluctuation is much weaker in this respect [36]. This is not an unusual phenomenon in multiparticle data, since the coarse fluctuation pattern arises from a small scale statistical noise, whereas a small number of events may contribute with very large scale fluctuations due to one or more dynamical effects. As we know, the degree of multifractality is usually quantified by the width of the spectrum $W = \alpha_{\max} - \alpha_{\min}$ at $f(\alpha_{\max}) = f(\alpha_{\min}) = 0$. If the calculated $f(\alpha)$ spectrum does not extend up to $f(\alpha) = 0$, as it is the case here, then the spectrum is extrapolated by an appropriate function to obtain the values of α for which $f(\alpha) = 0$. From this analysis we find $W = 1.55$ (experiment) and 1.31 (UrQMD+BEC). This is a direct evidence that the multifractality present in the experiment is stronger than that of the simulation. One can mention here that the MF-DMA method has been adopted here in multiparticle data analysis probably for the first time, therefore we could not compare the results of this analysis with similar other analysis for different colliding nuclei and/or energy involved. However the MF-DMA results presented here show a gross similarity with

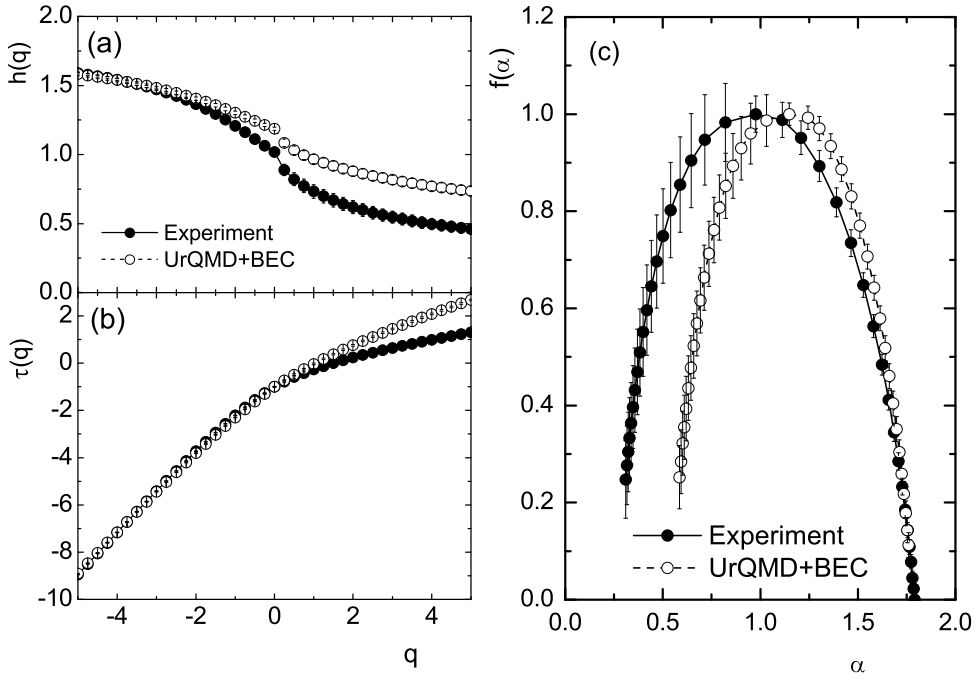

Figure 5.12: (a) Plot of $h(q)$ versus q, (b) $\tau(q)$ versus q, and (c) the singularity spectra obtained from the MF-DMA analysis with the window parameter $\theta = 0.5$. Line joining points are shown to guide the eye.

those obtained for a set of high multiplicity ($n_s \geqslant 150$) ^{32}S-Ag/Br events at 200A GeV [37]. In Fig. 5.13 the generalized fractal dimensions D_q are plotted against q. Following the trend we draw two separate diagrams, one for the experiment and another for the simulation. The D_q values obtained from all the other methods (G_q, T_q, SFM and MF-DFA) are included in the diagrams for an easy comparison. The D_q values measured from the conventional methods like G_q, T_q and SFM are all very close to the topological dimension of the supporting space. For the experiment all the D_q values decrease very slowly with increasing q, thereby indicating multifractality, whereas for the simulation the values are almost q independent. The detrended methods yield much smaller values of D_q over the interval $2 \leqslant q \leqslant 5$. According to the theory of fractals, the conventional G_q, T_q and SFM methods indicate the presence of a very low degree of multifractality in the data. The detrended methods contradict this observation and imply the existence of a strong multifractal structure of the data. Note that the SFM, G_q and T_q moment techniques are formulated particularly for the multiparticle data analysis, whereas the detrended method is formulated for the nonstationary time series data analysis. Therefore, the observed inconsistency between the detrended method and other conventional methods might be an outcome of the definitions of their moment generating functions, or it may so happen that the detrended method is not sensitive enough to the nature of fluctuation present in the multiparticle emission data, or the statistical component dominates the distribution to such an extent that in the detrended method it eventually suppresses the actual signal.

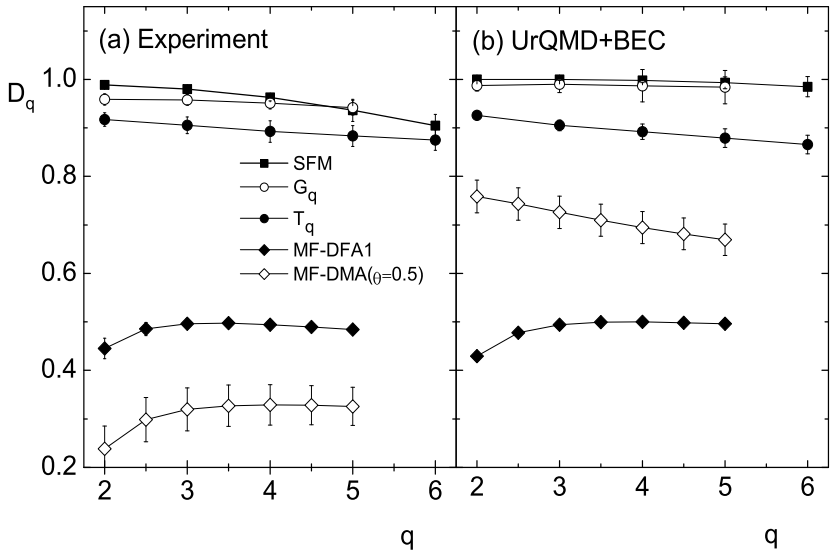

Figure 5.13: Generalized multifractal dimensions. The results of the MF-DMA (with $\theta = 0.5$) method are compared with those of the other methods. Lines joining points are drawn to guide the eye.

As mentioned, we have studied the event averaged values of the detrended multifractal variables. One can also extract the generalized Hurst exponent $h^{(e)}(q)$ from the single event detrended fluctuation function on an event-by-event basis, and can then take the average over the event sample [18], i.e.

$$\langle h(q) \rangle = \frac{1}{N_{ev}} \sum_{N_{ev}} h^{(e)}(q). \tag{5.40}$$

In this context we also study the difference between these two kinds of averaging of the $h(q)$ exponent, and find that the difference $\delta h(q) = h(q) - \langle h(q) \rangle$ marginally deviates from zero. That means, the detrended multifractal results presented here are not affected by one or the other averaging process adopted.

In the detrended analysis we select only the high multiplicity events with a multiplicity cut of $n_s \geqslant 50$. So the statistics of the samples reduce significantly, and it might influence the multifractal results. Therefore, we study the effects of the sample size on the results presented here. To do that, we consider a random number generated sample of 10,000 events. The multiplicity and pseudorapidity distributions of this sample are identical to those of the experiment (with a multiplicity cut $n_s > 50$). We calculate the generalized Hurst exponent $h^{\rm rand}(q)$ for the random number generated sample. The big sample is thereafter divided into ten smaller equal sized subsamples (1000 events in each) and the analysis is repeated for each of them. It is found that for the smaller subsamples the $h^{\rm rand}(q)$ values do not differ significantly (less than 6%) from each other as well as from the estimated value of the overall sample. In addition we have verified the sample size effect in the UrQMD+BEC generated

events. For this we divide the UrQMD+BEC sample, which is five times the experimental one, into five equal sized subsamples and redo the analysis individually for each of them. From this analysis also we have not noticed any substantial difference in the individual $h(q)$ values from those of the original UrQMD+BEC event sample. The entire exercise implies that the detrended multifractal results presented here are not significantly affected by the size of the sample statistics. Probably the key operation acting behind such a sample size independence of the multifractal exponent $h(q)$ is the averaging over the event sample. It is worth noting that in the case of time series data analysis the detrended multifractal results are quite sensitive to the length of the signal to be analyzed [8, 20].

5.6 Discussion

To summarize, we have presented some results on multifractal analysis of singly charged particles produced in ^{28}Si-Ag/Br interactions at 14.5A GeV. Specifically, we provide a multifractal characteristics of the pseudorapidity distribution of produced singly charged particles. Following the trend of our analysis the experimental results are systematically compared with a set of model simulation. The data behave expectedly and the results are consistent with those obtained from similar other experiments on AB interactions. The observations of this analysis can be summarized in the following way.

The multifractal moments introduced by Hwa [5] follow a scale invariant power-law and scale with diminishing phase space resolution size. The trend of the UrQMD+BEC (or UrQMD) simulated results are almost identical to the experiment. The intermittency results on the same sets of data, however, behave differently for the experiment and the simulations. Whereas, the self-similar nature of the $1d$ intermittency of the density fluctuation observed previously [21] is the primary motivation of the present work, where we have observed that the differences between experiment and simulations lie not in the scaling pattern of the multifractal moments, but in the quantitative aspects of the scaling parameters and in the derivatives thereof. The nature of multifractal mass exponent $\tau(q)$ or the Lipschitz-Hölder exponent α for the experiment cannot be distinguished from the simulations. The parameters themselves are probably not very sensitive to the nature of the fluctuation (statistical or dynamical) present in the data. However, when the statistical contribution is properly taken care of, we observe that within experimental uncertainties, the intermittency exponents ϕ_q overlap with the corresponding multifractal parameter (i.e., $q - 1 - \tau^{\rm dyn}(q)$). A small but definite departure from the simulations can be traced into the experiment, and the deviation slightly diminishes when BEC is incorporated into the UrQMD data. The multifractal spectrum, consistent in all aspects with its expected behavior, has a slightly smaller width in the UrQMD generated curve than that of the experiment and of the UrQMD+BEC. Therefore,

the multifractal spectrum might be considered as a sensitive variable that can distinguish the dynamical contribution from the statistical noise in the density fluctuation.

The stability index μ associated with the log-Lévy distribution is an important parameter that needs to be mentioned separately. Our intermittency analysis for the same sets of data resulted in a μ value that is way beyond its stability limit. In this analysis we have adopted a method based on the multifractal spectral function and, irrespective of the data set used, we have obtained different μ values in different q-regions. The estimated values of μ in the low-q region are consistent with the observation of our intermittency analysis, though the values are far above the upper acceptable limit $\mu = 2$ [24, 25]. However, in the high-q region the experimental μ value within errors is very close to the upper limit of the parameter. In any case the simulated values of μ deviate the experimental values to a large extent. Hence in the present case a log-Lévy distribution can not appropriately describe the multiplicity fluctuation.

Takagi's multifractal moments also exhibit expected power-law type of scaling behavior. Though Takagi's technique has a few advantages over Hwa's technique of analysis, the T_q moments are contaminated by statistical noise. This limitation is reflected in the multifractal parameters derived by using this method. The experimental D_q values obtained from the T_q moments are not significantly different from the corresponding simulated values. This is not true either for the factorial moment or for Hwa's moments, where the statistical noise has been taken care of at some level of analysis. However, a systematic deviation in D_q from the topological dimension which increases with order number, is an indication of the presence of multifractality in the single particle density distribution. The parameter D_q, unlike $\tau(q)$ and α, is found to be sensitive to the nature of fluctuation. The variation of D_q with $\ln q/(q-1)$ is consistent with the thermodynamic interpretation of the monofractal to multifractal phase transition, though the magnitude of specific heat does not corroborate any kind of universality as claimed in [31].

The detrended fluctuation functions for all the analyzed data also scale in a manner as expected from a multifractal system. The $h(q)$, $\tau(q)$ and $f(\alpha)$ obtained from the MF-DFA and MF-DMA analysis also confirm the presence of multifractality both in the experiment as well as in the simulations. The nature of these spectra and the estimated values of the Hurst exponent demand that the origin of fractality may be two, three or higher order particle correlation. The MF-DFA/MF-DMA prediction of the generalized fractal dimensions are consistently lower than that of the SFM method, Hwa's method and Takagi's method, the discrepancies being $\sim 50\%$. We also notice that except for the singularity spectrum and to a small extent the D_q values, within the error margins the experimental detrended multifractal parameters are not significantly different from the simulated values. The observations signify that the detrended technique like the other previously used techniques, is either probably

not sufficiently sensitive to the self-similar nature of fluctuation present in the data, or they lack an appropriate noise elimination technique. A reliable method of filtering out the statistical noise from the detrended fluctuation moments should therefore, be formulated to make the technique more effective.

Bibliography

[1] B. B. Mandelbrot, *The Fractal Geometry of Nature* (New York, Freeman, 1977).

[2] G. Paladin and A. Vulpiani, *Phys. Rep.* **156**, 147 (1987).

[3] P. Grassberger, I. Procaccia, *Physica* **D 13**, 34 (1984).

[4] T. C. Halsey *et al., Phys. Rev.* **A 33**, 1141 (1986).

[5] R. C. Hwa, *Phys. Rev.* **D 41**, 1456 (1990); *Phys. Rev.* **D 51**, 3323 (1995).

[6] R. C. Hwa and J. Pan, *Phys. Rev.* **D 45**, 1476 (1992).

[7] F. Takagi, *Phys. Rev. Lett.* **72**, 32 (1994).

[8] J. W. Kantelhardt *et al., Physica* **A 316**, 87 (2002).

[9] G.-F. Gu and W.X. Zhou, *Phys. Rev.* **E 82**, 011136 (2010).

[10] W. Florkowski and R. C. Hwa, *Phys. Rev.* **D 43**, 1548 (1991).

[11] C. B. Chiu and R. C. Hwa, *Phys. Rev.* **D 43**, 100 (1991).

[12] C. Albajar *et al.* (UA1 Collaboration), *Z. Phys.* **C 56**, 37 (1992).

[13] I. Derado, R. C. Hwa G. Jansco and N. Schmitz, *Phys. Lett.* **B 283**, 151 (1991).

[14] E. A. De Wolf, I. M. Dremin and W. Kittel, *Phys. Rep.* **270**, 1 (1996);
W. Kittel and E. A. De Wolf *Soft Multihadron Dynamics* (World Scientific, 2005).

[15] M. I. Adamovich *et.al.* (EMU01 Collaboration), *Europhys. Lett.* **44**, 571 (1998).

[16] D. Ghosh *et. al.*, *Phys. Rev.* **C 70**, 054903 (2004);
M. K. Ghosh, A. Mukhopadhyay and G. Singh, *J. Phys.* **G 32**, 2293 (2006);
S. Ahmad *et al., J. Phys.* **G 32**, 1279 (2006); *Nucl. Phys.* **A 780**, 206 (2006).

[17] J. Kwapień, P. Oświecimka and S. Drożdż, *Physica* **A 350**, 466 (2005);
E. Koscielny-Bunde *et al. J. Hydrology* **322**, 120 (2006);
S. Drożdż *et al., New Journal of Physics* **12**, 105003 (2010);
N. Cardenas, S. Kumar and S. Mohanty, *Appl. Phys. Lett.* **101**, 203702 (2012);
P. Mali, A. Mukhopadhyay, *Physica* **A 413**, 361 (2013); *Phys. Scr.* **90**, 035209 (2015);
P. Mali, *Theor. Appl. Climatol.*, **121**, 641 (2015).

[18] Y. X. Zhang, W. Y. Qian and C. B. Yang, *Int. J. Mod. Phys.* **A 23**(18), 2809 (2008).

[19] Y. Wang, C. Wu and Z. Pan, *Physica* **A 390**, 3512 (2011);
F. Wang, L. Wang and R.-B. Zou, *Chaos* **24**(3), 033127 (2014).

[20] P. Mali, *J. Stat. Mech.* 013201 (in press, 2016).

[21] P. Mali, A. Mukhopadhyay and G. Singh, *Can. J. Phys.* **89**, 949 (2011).

[22] P. Mali, A. Mukhopadhyay and G. Singh, *Acta Phy. Pol.* **B 43**, 463 (2012).

[23] J. Feder, *Fractals* (Plenum Press, New York, 1988).

[24] Ph. Brax and R. Peschanski, *Phys. Lett.* **B 253**, 255 (1991).

[25] W. Ochs, *Z. Phys.* **C 50**, 339 (1991).

[26] S. Hegyi, *Phys. Lett.* **B 318**, 642 (1993).

[27] A. Bialas and R. Peschanski, *Nucl. Phys.* **B 308**, 857 (1988).

[28] W. Ochs, *Phys. Lett.* **B 247**, 101 (1990).

[29] Y. Hu, M. Yu and L. Liu, *Chin. Phys. Lett.* **16**, 553 (1999).

[30] H. G. E. Hentschel and I. Proccacia, *Physica* **D 8**, 435 (1983).

[31] A. Bershadski, *Phys. Rev.* **C 59**, 364 (1999).

[32] C. V. Chianca, A. Ticona and T.J.P. Penna, *Physica* **A 357**, 447 (2005).

[33] C. -K. Peng *et el., Phys. Rev.* **E 49**, 1685 (1994).

[34] S. M. Ossadnik *et al., Biophys. J.* **67**, 64 (1994).

[35] P. Mali, S. Sarkar, S. Ghosh, A. Mukhopadhyay, G. Singh, *Physica* **A 424**, 25 (2015).

[36] S. Drożdż, P. Oświęcimka, *Phys. Rev.* **E 91**, 030902(R) (2015).

[37] P. Mali, A. Mukhopadhyay and G. Sing, *Physica* **A** (in press, 2016).